Chaotic Modeling and Simulation (CMSIM) 3: 305–318, 2018

The geometry of transition states: How invariant manifolds determine reaction rates

F. Revuelta[1,2], Thomas Bartsch[3], R. M. Benito[1], and F. Borondo[2,4]

[1] Grupo de Sistemas Complejos, Escuela Técnica Superior de Ingeniería Agronómica, Alimentaria de Biosistemas, Universidad Politécnica de Madrid, Avda. Complutense s/n, 28040 Madrid, Spain
(E-mail: fabio.revuelta@upm.es, rosamaria.benito@upm.es. orchid.org/0000-0002-2410-5881, orchid.org/0000-0003-3949-8232)
[2] Instituto de Ciencias Matemáticas (ICMAT), Cantoblanco, 28049 Madrid, Spain
[3] Centre for Nonlinear Mathematics and Applications, Department of Mathematical Sciences, Loughborough University, Loughborough LE11 3TU, United Kingdom
(E-mail: T.Bartsch@lboro.ac.uk)
[4] Departamento de Química, Universidad Autónoma de Madrid, Cantoblanco, 28049 Madrid, Spain
(E-mail: f.borondo@uam.es)

Abstract. Over the last years, a new geometrical perspective on transition state theory has been developed that provides a deeper insight on the reaction mechanisms of chemical systems. This new methodology is based on the identification of the invariant structures that organize the dynamics at the top of the energetic barrier that separates reactants and products. Moreover, it has allowed to solve, or at least circumvent, the *recrossing-free problem* in rate calculations. In this paper, we will discuss which kind of objects determine the reaction dynamics in the presence of dilute, dense and condensed phase baths.
Keywords: Transition state theory, invariant manifolds, Langevin, friction, white noise, colored noise, memory, correlation, molecular systems, rates.

1 Introduction

The rate at which some substances (reactants) are combined to produce others (products) has always been a central problem for chemists. For this purpose, the correct identification of reactive trajectories is crucial. Numerical simulations, like all-atom molecular dynamics, provide suitable methodologies for this task, but they are usually time consuming due to the large number of interacting particles whose dynamics must be computed. Transition State Theory (TST) provides an alternative way to calculate chemical rates that is simple and accurate. Though initially proposed to study chemical reactions of small molecules, TST has been later applied to other fields of science, like celestial mechanics [1] or atomic ionization [2], among others.

Received: 4 November 2017 / Accepted: 24 March 2018

ISSN 2241-0503

In many reactions reactants and products are separated by an energetic barrier. The crossing of this barrier is the most critical step for the reaction to take place; it acts as a *bottleneck* in phase space. Traditional TST assumes the existence of a dividing surface (DS) between reactants and products that is free of recrossings, i.e., a surface that is crossed once and only once by all reactive trajectories. This DS is usually placed at the top of the energetic barrier. The fundamental challenge in TST is adequatelly identifying such an optimal recrossing-free DS, particularly in systems strongly coupled to their surrounding environment. For this purpose, *variational TST*, determines the DS by minimizing the number of recrossings [3].

Over the last years, TST has been extended by shifting the focus from the calculation of a DS to the identification of the invariant structures that organize the dynamics close to the barrier top. This new geometrical perspective has provided a better understanding of the reaction mechanism as well as alternative ways to reliably identify reactive trajectories and perform rate calculations in externally driven systems. In this paper we will review some of these recent advances from a unified point of view, which allows us to highlight the fundamental ideas that underly seemingly disparate developments.

First, in Sec. 2 we discuss the reaction mechanism for reactions in gas phase, where coupling to the environment is negligible. Section 3 is devoted to solvated systems that are strongly coupled to a bath characterized by a white noise force. Then, in Sec. 4 we describe the flux-over-population method that provides a well-established framework for a rate calculation. The extension of the previous results to correlated noise is briefly discussed in Sec. 5. Finally, we conclude the paper in Sec. 6 with a short summary.

2 Autonomous reactions in the gas phase

The interaction with the environment in dilute gas phase reactions is usually so small that it can simply be neglected. As a consequence, the dynamics of the system is conservative to a good approximation and can be described in a Hamiltonian framework.

Let us consider for simplicity a system with 2 degrees-of-freedom (dof) and an energetic barrier, with a saddle point at position $\boldsymbol{q}^{\mathrm{SP}} = 0$. The corresponding phase space is then 4 dimensional, but all dynamics takes place in the three dimensional volume confined by the energy shell $E = U(\boldsymbol{q})$. A necessary condition for a trajectory to react is that its energy exceeds the saddle point energy. This energy shell is represented in grey for two characteristic settings in Fig. 1. As can be seen in Fig. 1(a), the energy surface is divided in two disconnected parts if the energy is smaller than the energy, $U^{\mathrm{SP}} = U(\boldsymbol{q}^{\mathrm{SP}})$. All in all, a given initial condition can react, i.e., move from the reactant region into the product region, only if its energy exceeds U^{SP}. If that happens, the energy surface connects the reactant (left) and product regions (right), as shown in Fig. 1(b). However, this is only a necessary but not a sufficient condition.

In the system under study, the natural choice for a DS is such that it is placed at the barrier top, where a bottleneck is formed, as shown in Fig. 1(b). By shifting this surface, Pechukas and Pollak [4] demonstrated that the DS

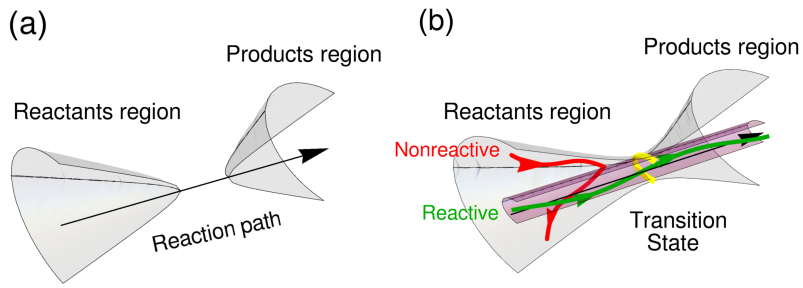

Fig. 1. Phase space of a system with two degrees of freedom. (a) For low energies, the energy surface (grey) is divided in two disconneted regions (one for products and the other one for reactants), and then there are no reactive trajectories. (b) When the energy is larger than that of the saddle point that sits on the top of the energetic barrier, the reaction can take place. Reactive trajectories (like the green one) are only those that lie inside the invariant manifolds (purple tubes), while those outside (like the red one) do not react. The invariant manifolds are connected along the unstable periodic orbit on the barrier top (yellow semicircle).

that minimizes the reactive flux is an unstable periodic orbit called *Periodic Orbit Dividing Surface (PODS)* and that the action of the PODS equals the reactive flux (14). Furthermore, the PODS is a strictly recrossing-free DS and yields the exact classical reaction rate if it is the only periodic orbit in the barrier region [5].

The reactivity of the system is determined by the invariant manifolds that emerge from the PODS [6–8]. The stable and unstable manifolds of the PODS consist of all those trajectories that asymptotically approach the PODS for large positive or negative times, respectively. They are topologically cylinders: The motion around the PODS, which appears as a circle in phase space, is combined with the motion towards or away from the PODS. These cylinders are often called *reaction tubes* because all initial conditions starting inside the stable cylinder (like the green trajectory in Fig. 1) will cross the saddle to the other side and leave the barrier region through the unstable cylinder. Trajectories outside the stable cylinder will not cross the barrier.

Similar structures exist in the phase space of a higher-dimensional Hamiltonian system with f dof near a saddle point of the potential energy [2,9,10] and for energies not too high above the saddle point energy. The PODS is then replaced by an invariant (hyper-)sphere of dimension $2f-3$ called a *Normally Hyperbolic Invariant Manifold (NHIM)*. Its associated stable and unstable cylinders have dimension $2f-2$. As in the 2-dof case, they divide the energy shell into a reactive interior and a non-reactive exterior. All these objects can be computed using normal form theory (see, e.g., Ref. [2]).

3 Reactions in stochastically driven systems

In most chemical reactions, the reactive system is strongly coupled to its environment. In principle, of course, the system could still be described within the

formalism of the preceeding section if the system and all the particles of the environment were considered as part of an *extended* system. However, this unified system would have so many dof (of the order of Avogadro constant), that this approach is rarely feasible. Alternatively, one can describe the influence of the bath phenomenologically through an external force, which depending on the nature of the environment can either be deterministically prescribed, as, e.g., the force exerted by a laser field [11,12], or can be randomly fluctuating, as in a solvent. For the sake of simplicity and brevity, we will restrict the discussion to one dimensional barriers. The interested reader can find further details and a discussion for higher dimensional barriers in Refs. [13–17].

3.1 Langevin model for reactions in thermalized baths

The equation of motion for a reactive system driven by a thermalized bath is well described by the Langevin equation [18], one of the most famous models for stochastic systems. This equation is given by

$$m\ddot{x} = -\frac{dU(x)}{dx} - m\gamma\dot{x} + \xi(t), \tag{1}$$

where x is the reaction coordinate, $U(x)$ is the potential energy of the system, or the potential of mean force in the case of a fluctuating environment, and γ is a friction constant. Though this is not indicated in the notation, the external force $\xi(t)$ can also depend on the system coordinate x or velocity $\dot{x}$. In our case, however, we will assume that the fluctuating external force $\xi = \xi_\alpha(t)$ depends on a realization α of some random noise, following a Gaussian distribution with zero mean. The strength of the random force is related to the friction constant by the fluctuation-dissipation theorem

$$\langle \xi_\alpha(t)\xi_\alpha(t')\rangle_\alpha = 2k_{\mathrm{B}}Tm\gamma\,\delta(t-t'), \tag{2}$$

where $\langle \dots \rangle_\alpha$ denotes an average over the noise.

It is often useful to expand the potential U around the saddle point $x^{\mathrm{SP}} = 0$ as

$$U(x) = -\frac{1}{2}m\omega_b^2 x^2 + m\frac{c_3}{3}x^3 + m\frac{c_4}{4}x^4 + \dots, \tag{3}$$

and separate the harmonic (quadratic) part from the higher orders. (Note that $\omega_b^2 > 0$ because U has a maximum, not a minimum, at x^{SP}.) If we rewrite Eq. (1) as a system of differential equations in phase space with coordinates x and $v = \dot{x}$ and introduce the new coordinates

$$z_i = \frac{v - \lambda_j x}{\lambda_j - \lambda_i}, \tag{4}$$

where $i, j = 0, 1$, $j \neq i$, and $\lambda_i = -\frac{1}{2}\left[\gamma - (-1)^i\sqrt{\gamma^2 + 4\omega_b^2}\right]$, the equation of motion (1) takes the form

$$\dot{z}_i = \lambda_i z_i + \frac{f(z_0 + z_1)}{\lambda_i - \lambda_j} + \frac{1}{\lambda_i - \lambda_j}\,\xi(t), \tag{5}$$

where $f(x) = m\omega_b^2 x - U'(x) = -c_3x^2 - c_4x^3 - \ldots$ gathers the anharmonic terms of the mean force. Equations (5) decouple for a hamonic barrier, $f = 0$, and it becomes visible that the λ_i are the eigenvalues of the linearized dynamics near the stationary point. Because $\lambda_0 > 0$ and $\lambda_1 < 0$, the coordinate z_0 corresponds to an unstable direction in phase space whereas z_1 corresponds to a stable direction.

3.2 The transition state trajectory

An immediate consequence of the influence of the environment is that the energy of the reactive system is not conserved. Therefore, it does not make sense to discuss the phase space structure at a fixed energy, as it was done in Sec. 2, that may vary for different energies. Instead, there is a single set of invariant objects near the saddle point that is to be discovered.

A second consequence of the external driving is that the equilibrium point on top of the barrier disappears: The system can no longer be at rest on the barrier top and remain there, as it could in the Hamiltonian case. It might appear that thereby the foundation for the construction of invariant structures, as it was carried out for gas phase reactions, is undermined. To overcome this difficulty, an invariant structure must be found that can replace the equilibrium point. The crucial idea [13,19,20] is to identify a trajectory, called the Transition State (TS) trajectory, that remains in the vicinity of the barrier for all time, without ever descending into either the reactant or the product wells.

The exact nature of the TS trajectory and the method of its calculation depend, of course, on the details of the external driving. Its existence can nevertheless be shown for a large class of systems. In the simplest case, the external driving is periodic in time, which renders a TS trajectory that is an unstable periodic orbit [11,12].

For any type of external driving, the TS trajectory can easily be constructed if the barrier is harmonic, i.e., $f(x) = 0$. The equations of motion (5) can in this case be solved by

$$z_i(t) = C_i e^{\lambda_i t} + \frac{1}{\lambda_i - \lambda_j} S[\lambda_i, \xi; t], \tag{6}$$

where C_i are arbitrary constants and the S-functionals [13,21] are given by

$$S[\lambda, g; t] = \begin{cases} -\displaystyle\int_t^\infty g(t') \exp(\lambda(t - t'))\, dt', & \text{if } \operatorname{Re}\lambda > 0, \\ +\displaystyle\int_{-\infty}^t g(t') \exp(\lambda(t - t'))\, dt', & \text{if } \operatorname{Re}\lambda < 0. \end{cases} \tag{7}$$

(We assume for the sake of simplicity that $\operatorname{Re}\lambda_i \neq 0$, i.e., the friction constant γ is non-zero. For the case of driven Hamiltonian systems with $\operatorname{Re}\lambda_i = 0$, see Ref. [21].) Because the exponential terms in Eq. (6) diverge exponentially as $t \to +\infty$ (for z_0) or $t \to -\infty$ (for z_1), a trajectory that remains near the origin can only be obtained by setting $C_i = 0$, which gives rise to the TS trajectory

$$z_i^\ddagger(t) = \frac{1}{\lambda_i - \lambda_j} S[\lambda_i, \xi; t]. \tag{8}$$

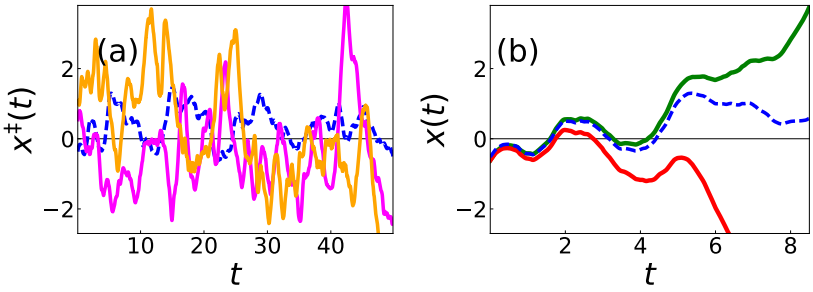

Fig. 2. Time-evolution of different characteristic trajectories. (a) The transition state trajectories for different noise ensembles and $k_{\mathrm{B}}T = 1$ (dashed blue), $k_{\mathrm{B}}T = 5$ (magenta), and $k_{\mathrm{B}}T = 10$ (orange) always fluctuate around the saddle point position, $x^{\mathrm{SP}} = 0$. (b) Typical trajectories descend from the saddle quickly. A reactive trajectory (green) crosses the transition state trajectory (dashed blue) once. A non-reactive trajectory (red) does not cross the transition state trajectory.

The TS trajectory on an anharmonic barrier can be obtained by writing

$$z_i(t) = z_i^{\ddagger}(t) + \Delta z_i(t),$$

where $\Delta z_i(t)$ denotes the deviation of the exact TS trajectory from its harmonic approximation (8). It satisfies the equations of motion

$$\Delta \dot{z}_i = \lambda_i \Delta z_i + \frac{f(x^{\ddagger} + \Delta z_0 + \Delta z_1)}{\lambda_i - \lambda_j} \tag{9}$$

with the position $x^{\ddagger}(t) = z_0^{\ddagger}(t) + z_1^{\ddagger}(t)$ the position of the harmonic TS trajectory. Equations (9) can be solved formally by

$$\Delta z_i(t) = \frac{1}{\lambda_i - \lambda_j} \, S\left[\lambda_i, f(x^{\ddagger} + \Delta z_0 + \Delta z_1);\ t\right]. \tag{10}$$

This is only a formal solution because the unknown functions Δz_i appear in the S-functional on the right hand side. Nevertheless, because the Δz_i appear only through the anharmonic force f that is small near the barrier, Eq. (10) provides a suitable basis for a numerical scheme. If the harmonic approximation $\Delta z_0 = \Delta z_1 = 0$ is substituted into the right hand side of Eq. (10), the S-functionals can be evaluated to yield an improved approximation for the Δz_i. The new approximation can then be substituted into the right hand side again, and the process iterated to convergence. This process has successfully been used to obtain the TS trajectory on strongly anharmonic potentials for periodic, quasiperiodic and stochastic driving [12].

Figure 2(a) shows the TS trajectory for a harmonic barrier under stochastic driving. The TS trajectories have been samples for three different noise sequences at three different temperatures. As expected from Eq. (8), the dynamics of the TS trajectory depends strongly on the noise sequence α. Moreover, the amplitude of the oscillations increases with the temperature. In any

case, the TS trajectory remains "jiggling" in the vicinity of the barrier top. Let us remark that, as it randomly moves, it also displaces its invariant manifolds, which organize the dynamics in the barrier top as will be discussed in the next subsection. By contrast, as shown in Fig. 2(b), a generic reactive (nonreactive) trajectory quickly dives into the product (reactant) side, defined by $x > 0$ ($x < 0$). Notice that these trajectories cross the naive DS $x^{\mathrm{SP}} = 0$ many times, but TS trajectory. This fact can be explained because of their different velocities, as will be reported below.

3.3 Time-dependent invariant manifolds

Having identified the TS trajectory that corresponds to the equilibrium point or the NHIM in an autonomous Hamiltonian system in that it is bound to the neighborhood of the barrier for all times, we now turn to an investigation of the phase space structures that surround it. To this end, consider once again the relative coordinates

$$\Delta z_i = z_i - z_i^{\ddagger} \tag{11}$$

with the harmonic TS trajectory $z_i^{\ddagger}$. The relative coordinates satisfy the equations of motion (9) but their interpretation is now different from what was used in Sec. 3.2. They represent a typical trajectory in the barrier region, away from the TS trajectory.

Notice that the dynamics of the relative coordinate described by Eq. (9) does not depend explicitly on the noise, but it does implicitly through the coordinate $x^{\ddagger}$ of the TS trajectory. Moreover, the two equations of motion decouple in the harmonic approximation, i.e., if $f(x) = 0$. In that case, their solution is given by

$$\Delta z_i(t) = \Delta z_i(0)\, e^{\lambda_i t}, \tag{12}$$

The lines $\Delta z_0 = 0$ and $\Delta z_1 = 0$ are invariant under dynamics, as any initial condition with $\Delta z_0(0) = 0$ or $\Delta z_1(0) = 0$ satisfies $\Delta z_0(t) = 0$ or $\Delta z_1(t) = 0$, respectively, for all times. In fact, these lines are the invariant manifolds associated with the TS trajectory. In particular, $\Delta z_0 = 0$ defines the stable manifold, because every initial condition with $\Delta z_0(0) = 0$ will asymptotically approach the origin, i.e., the TS trajectory, as $\lambda_1 < 0$. Similarly, $\Delta z_1 = 0$ determines the unstable manifold because any initial condition $\Delta z_1(0) = 0$ will move away from the origin as $t \to \infty$, but it will approach the origin as $t \to -\infty$, since $\lambda_0 > 0$.

Figure 3(a) sketches the harmonic approximation to the stable and unstable manifolds in relative coordinates along with four typical trajectories. As in a Hamiltonian system, the latter fall into four distinct classes, depending on whether they originate on the reactant or product side of the barrier in the remote past and whether they end on the reactant or product side in the distant future. As can be seen, the invariant manifolds form the boundary between phase space regions with qualitatively different behavior. For our present purposes, we will only study the future behavior of trajectories and call trajectories reactive or nonreactive if they move to products or reactants,

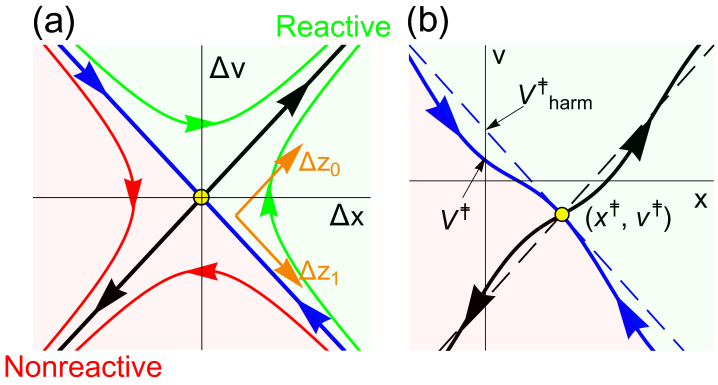

Fig. 3. Phase space view of the time-dependent invariant manifolds of the Langevin equation (1). (a) The invariant manifolds are time-independent in the harmonic approximation and in relative coordinates. (b) In space-fixed coordinates, the invariant manifolds are attached to the transition state trajectory (yellow dot) and move through phase space with it. In any case, all trajectories above the stable manifold are reactive (green), while those below are nonreactive (red). For initial conditions with $x = x^{\mathrm{SP}} = 0$, trajectories with velocities above a critical value $V^{\ddagger}$ are reactive (see Sec. 4).

respectively. This distinction can be made with the help of the stable manifold: all initial conditions that lie below the stable manifold are nonreactive, while those above the stable manifold are reactive.

The phase space structure that has so far been described in relative coordinates can now be transferred to space-fixed coordinates x and v, in which the origin $\Delta x = \Delta v = 0$ of the relative coordinates is identified with the TS trajectory $x^{\ddagger}, v^{\ddagger}$ and is time-dependent. Therefore, the invariant manifolds, indicated by dashed lines in Fig. 3(b), move through phase space with the TS trajectory, but they retain their function: They still separate reactive from non-reactive trajectories. In particular, a knowledge of the instantaneous position of the stable manifold allows one to predict with certainty whether a trajectory will be reactive.

Figure 3 also shows that the time-dependent DS $\Delta x = 0$ or $x = x^{\ddagger}$ will be recrossing free, as was indicated already in Fig. 2(b).

If the barrier is anharmonic, the invariant manifolds are distorted, as shown in Fig. 3(b). Their shape, as well as their location, will depend on time and on the details of the external driving. Still, if the anharmonicity is not too large, they survive [22] and keep on acting as separatrices for reactivity.

The TS trajectory as well as the associated invariant manifolds can be computed by normal form theory. For stochastically driven systems this was carried out in Ref. [23–26]. These calculations provide full detail of the phase space structure. As will be described below, for specific purposes, such as rate calculation, it can be advantageous to use a specialized computational scheme that provides the information of immediate interest at significantly reduced computational cost.

4 Reactions in white noise

We will now discuss how the phase space structures described so far can be used in the calculation of reaction rates. The details of such a calculation depend, of course, on the precise setup of the system under study and on the definition of the rate constant.

A common setup in which to study a thermally activated crossing of an energy barrier is to assume that particles that have crossed the barrier and progressed sufficiently far to the product side are removed there, while at the same time particles are replaced on the reactant side with low energy and at a sufficient distance from the barrier. For sufficiently long time, a stationary state will be established in which there is a steady flux of particles from the reactant to the product side. A reaction rate for this situation was first derived by Kramers [27]. The interested reader is referred to Ref. [18] for a review of the extensive literature in the field.

The reaction rate can be computed through the flux-over-population expression given by

$$k = \frac{J}{N}, \tag{13}$$

where N is an average population of the reactant region and

$$J = \langle v\chi_r(v)\rangle_{\alpha,\mathrm{IC}} \tag{14}$$

is the reactive flux out of that region. Here v is the velocity, and $\langle\ \rangle_{\alpha,\mathrm{IC}}$ denotes an average over interactions with the environment, α, and an ensemble of initial conditions (IC) that are in thermal equilibrium following the Boltzmann distribution $p(x,v) = \delta(x - x^{\mathrm{SP}}) \exp\left[-v^2/(2mk_{\mathrm{B}}T)\right]$ being m the particle mass.

The characteristic function $\chi_r(v)$ in Eq. (14) encodes all the complexity of the reaction mechanism and determines which trajectories must be incorporated in the reactive flux; this function equals 1 if the trajectory is reactive, and 0 otherwise. The simplest approximation to this function is yielded by TST, which assumes that every trajectory with positive velocity reacts, i.e., $\chi_r^{\mathrm{TST}}(v) = 1$ if $v > 0$, and 0 otherwise. Unfortunately, this assumption is usually violated. Then TST overestimates the true reactive flux, and consequently the reaction rate (13). The accuracy of the TST prediction can be quantified through the transmission factor given by

$$\kappa = \frac{k}{k^{\mathrm{TST}}} \leq 1, \tag{15}$$

which gives the ratio between the true rate k and the TST prediction k^{TST} obtained using the previous characteristic function χ_r^{TST}. Equation (15) has rather simple form but its numerical evaluation can be computationally demanding as one must take averages over several interactions with the environment and over several initial conditions to asses which trajectories are reactive and which ones are not, by solving the equations of motion of the system until their energies lie far below the barrier top.

However, as the phase space plot in Fig. 3(b) shows, once the initial position $x = x^{\mathrm{SP}} = 0$ of the initial ensemble has been fixed, there is a critical velocity

$V^\ddagger$ such that trajectories with initial velocities larger than $V^\ddagger$ are reactive, those with smaller velocities are nonreactive. In terms of the critical velocity, the characteristic function can be expressed *exactly* as

$$\chi_r(v) = \begin{cases} 1, & \text{if } v > V^\ddagger, \\ 0, & \text{if } v < V^\ddagger. \end{cases} \tag{16}$$

The critical velocity $V^\ddagger$ depends on the realization α of the noise.

By substituting the characteristic function (16) into the flux formula (14), one obtains the transmission factor [20,14–16]

$$\kappa = \left\langle e^{-\frac{mV^{\ddagger\,2}}{2k_\mathrm{B}T}} \right\rangle_\alpha . \tag{17}$$

Equation (17) reduces the problem of rate calculation to a computation of the critical velocity. As shown in Refs. [14,15], the perturbative scheme that was used in Sec. 3.2 to obtain the TS trajectory can be adapted to this purpose. It yields an expansion of the critical velocity in powers of $\sqrt{k_\mathrm{B}T}$, gives rise to an expansion of the transmission factor in powers of $k_\mathrm{B}T$. For a general one-dimensional potential (3), the leading terms are given by

$$\kappa = \mu - \frac{\mu}{6}\frac{c_3^2\,k_\mathrm{B}T}{\omega_b^6}\left(\frac{1-\mu^2}{1+\mu^2}\right)^2 \frac{10\mu^4+41\mu^2+10}{2\mu^4+5\mu^2+2} + \frac{3}{4}\frac{c_4 k_\mathrm{B}T\gamma^2}{\omega_b^3\lambda_1(\lambda_0-\lambda_1)^2}, \tag{18}$$

where $\mu = \lambda_0/\omega_b$ is Kramers's famous result for harmonic barriers [27]. This result was first obtained, for white and correlated noise, in Ref. [28,29], and by the present method in [14,15]. The geometric approach using invariant manifolds can be extended to multidimensional systems and to systems driven by correlated noise, as described in Refs. [14–17], where the perturbative rate formulas are also compared to the results of numerical simulation.

5 Reactions in correlated noise

5.1 The generalised Langevin equation

The Langevin equation (1) assumes that the bath thermalizes infinitely fast. This is, however, not the case of liquid phase reactions. Consequently, a more realistic description of the bath must also take into account the finite-time dynamics and the underlying correlations. For this purpose, the generalized Langevin equation

$$m\ddot{x} = -\frac{dU(x)}{dx} - m\int_{-\infty}^{t} \gamma(t-t')\,\dot{x}(t')\,dt' + m\,R_\alpha(t), \tag{19}$$

provides an excellent benchmark. In this equation, $U(x)$ represents again the potential given by Eq. (3), and $\gamma(t)$ is the friction kernel. In our case, this friction kernel will be taken exponential as in many realistic chemical reactions [30]. Mathematically,

$$\gamma(t) = (\gamma_0/\tau)\,e^{-t/\tau}, \tag{20}$$

where τ is a characteristic correlation time and γ_0 a damping strength. Notice that in the white noise limit, where $\tau \to 0$, the friction kernel becomes Markovian, $\gamma(t) \equiv \gamma_0$, and then Eq. (19) reduces to Eq. (1). Finally, $R_\alpha(t)$ is the fluctuating Gaussian colored noise force exerted by the heat bath. Let us remark that $\gamma(t)$ and $R_\alpha(t)$ are related to each other according to the fluctuation-dissipation theorem, which in this case reads

$$\langle R_\alpha(0) R_\alpha(t) \rangle_\alpha = \frac{k_\mathrm{B} T\, \gamma(t)}{m}. \tag{21}$$

Equation (19) is a second order differential equation, which can be rewritten as a system of two first order differential equations. Still, the calculation of a solution is complicated because of the integral from infinitely far past. Nevertheless, this last integral can be avoided by addying the new variable [31–34],

$$\zeta = -\int_{-\infty}^{t} \gamma(t-s)\, \dot{x}(s)\, ds, \tag{22}$$

and subtituting Eq. (19) by the system of equations

$$\dot{x} = v, \qquad \dot{v} = -\frac{1}{m}\,\frac{\partial U(x)}{\partial x} + \zeta, \qquad \dot{\zeta} = -\frac{\gamma_0}{\tau}\, v - \frac{1}{\tau}\,\zeta + \xi_\alpha(t), \tag{23}$$

which defines an extended phase space of dimension three instead of two, being ξ_α a white noise source that satisfies the fluctuation–dissipation theorem

$$\langle \xi_\alpha(t) \xi_\alpha(s) \rangle_\alpha = \frac{2 k_\mathrm{B} T\, \gamma_0}{m \tau^2}\, \delta(t-s). \tag{24}$$

5.2 Invariant manifolds in correlated noise

In the presence of colored noise, an expression for the TS trajectory similar to that given by Eq. (8) can be also obtained. Note that this TS trajectory has three components instead of just two as in the white noise setting.

To study the dynamics in the vicinity of the TS, we use again relative coordinates as in Eq. (11), yielding

$$\Delta \dot{z}_i = \lambda_i \Delta z_i + K_i\, f(x), \tag{25}$$

being K_i some constants (see Refs. [16,17]). As in the white noise setting, the three Eqs. (25) decouple in the harmonic limit. Their solution is again given by Eq. (12). However, in this case we have one unstable direction, that parallel to the eigenvector associated with λ_0, and two stable ones, corresponding to the eigenvectors for λ_1 and λ_2. Consequently, the stable manifold is in this case given by the plane defined by the two stable eigenvectors, as shown in Fig. 4(a).

The calculation of the stable and unstable manifolds becomes much more involved if the barrier presents anharmonicities. Still, dynamical systems theory assures that they exist as long as the anharmonicities are not too large [22]. As in the white noise limit, the invariant manifolds do not only move randomly

attached to the TS trajectory but get also stochastically deformed in the presence of anharmonicities, as shown in Fig. 4(b). In any case, they allow us to correctly predict which trajectories will end up in the product side: only those that lie above the stable manifold. Moreover, they can be used to generalize Eq. (18) to obtain a transmission factor for colored noise that does also account for the barrier anharmonicities, which extends Grote-Hynes theory to this more involved situation following an alternative methodology from other previous studies [28]. The validity of the previous extension has been demonstrated through extensive numerical simulations, both in model potentials [17], as well as in a realistic molecule, the LiNC/LiCN isomerizing system [16].

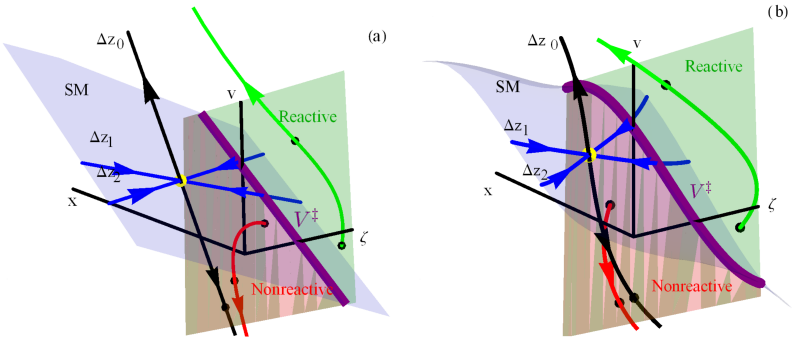

Fig. 4. Extended phase space of the generalized Langevin equation (19) for harmonic (a) and anharmonic (b) potential barrier. Yellow dot: instantaneous position of the transition state trajectory. Black curve: unstable manifold. Light blue surface and trajectories within: stable manifold (SM). The dividing surface (v–ζ plane) is partitioned into reactive (green) and nonreactive (brown) regions by the intersection of the dividing surface with the stable manifold and defines the critical velocity $V^\ddagger = V^\ddagger(\zeta)$ (purple). Representative reactive (green) and nonreactive (red) trajectories intersect the dividing surface as indicated by black dots.

6 Summary

Over the last two decades, transition state theory has experienced a tremendous advance because of the application of new mathematical tools to study chemical reactions. These new methodologies are based on the correct identification of the geometrical structures —the invariant manifolds— that determine the dynamics in the transition state, and then the reactivity of the system. More importantly, they can be used to predict if an initial condition renders a reaction or not, a task that is particularly demanding when the system is strongly coupled to a bath. Moreover, they can be used to obtain explicit expressions for the reaction rate without the need of any reference dividing surface.

Acknowledgments

The research leading to these results has received funding from the Ministerio de Economía y Competitividad under Contracts MTM2015-63914-P and ICMAT Severo Ochoa under SEV-2015-0554, and from the European Union's Horizon 2020 research and innovation programme under grant agreement No. 734557.

References

1. Charles Jaffé, Shane D. Ross, Martin W. Lo, Jerrold Marsden, David Farrelly, and T. Uzer. Statistical theory of asteroid escape rates. *Phys. Rev. Lett.*, 89:011101, Jun 2002.
2. T. Uzer, C. Jaffé, J. Palacián, P. Yanguas, and S. Wiggins. The geometry of reaction dynamics. *Nonlinearity*, 15(4):957–992, July 2002.
3. Bruce C. Garrett and Donald G. Truhlar. Variational transition state theory. In Clifford E. Dykstra, Gernot Frenking, Kwang S. Kim, and Gustavo E. Scuseria, editors, *Theory and Applications of Computational Chemistry: The First Forty Years*, chapter 5, pages 67–87. Elsevier, 2005.
4. Eli Pollak and Philip Pechukas. Transition states, trapped trajectories, and classical bound states embedded in the continuum. *J. Chem. Phys.*, 69(3):1218–1226, August 1978.
5. Philip Pechukas and Eli Pollak. Classical transition state theory is exact if the transition state is unique. *J. Chem. Phys.*, 71(5):2062–2068, September 1979.
6. A M Ozorio de Almeida, N de Leon, Manish A Mehta, and C Clay Marston. Geometry and dynamics of stable and unstable cylinders in Hamiltonian systems. *Physica D: Nonlinear Phenomena*, 46(2):265–285, November 1990.
7. N de Leon, Manish A Mehta, and Robert Q Topper. Cylindrical manifolds in phase space as mediators of chemical reaction dynamics and kinetics. I. Theory. *The Journal of Chemical Physics*, 94(12):8310–8328, June 1991.
8. N de Leon, Manish A Mehta, and Robert Q Topper. Cylindrical manifolds in phase space as mediators of chemical reaction dynamics and kinetics. II. Numerical considerations and applications to models with two degrees of freedom. *The Journal of Chemical Physics*, 94(12):8329–8341, June 1991.
9. H. Waalkens, A. Burbanks, and S. Wiggins. A computational procedure to detect a new type of high-dimensional chaotic saddle and its application to the 3D Hill's problem. *J. Phys. A*, 37(24):L257–L265, June 2004.
10. Holger Waalkens, Andrew Burbanks, and Stephen Wiggins. Phase space conduits for reaction in multidimensional systems: HCN isomerization in three dimensions. *J. Chem. Phys.*, 121(13):6207–6225, October 2004.
11. Galen T Craven, Thomas Bartsch, and Rigoberto Hernandez. Persistence of transition-state structure in chemical reactions driven by fields oscillating in time. *Physical Review E*, 89:040801(R), 2014.
12. F. Revuelta, Galen T. Craven, Thomas Bartsch, R. M. Benito, F. Borondo, and Rigoberto Hernandez. Transition state theory for activated systems with driven anharmonic barriers. *J. Chem. Phys.*, 147(7):074104, 2017.
13. Thomas Bartsch, Rigoberto Hernandez, and T. Uzer. Transition state in a noisy environment. *Phys. Rev. Lett.*, 95(5):058301, July 2005.
14. F. Revuelta, Thomas Bartsch, R. M. Benito, and F. Borondo. Communication: Transition state theory for dissipative systems without a dividing surface. *J. Chem. Phys.*, 136(9):091102, March 2012.

15. Thomas Bartsch, F. Revuelta, R. M. Benito, and F. Borondo. Reaction rate calculation with time-dependent invariant manifolds. *J. Chem. Phys.*, 136(22):224510, June 2012.
16. F. Revuelta, Thomas Bartsch, P. L. Garcia-Muller, Rigoberto Hernandez, R. M. Benito, and F. Borondo. Transition state theory for solvated reactions beyond recrossing-free dividing surfaces. *Phys. Rev. E*, 93:062304, June 2016.
17. Thomas Bartsch, F. Revuelta, R. M. Benito, and F. Borondo. Finite-barrier corrections for multidimensional barriers in colored noise, 2017. In press.
18. Peter Hänggi, Peter Talkner, and Michal Borkovec. Reaction-rate theory: fifty years after Kramers. *Rev. Mod. Phys.*, 62(2):251–341, April 1990.
19. Thomas Bartsch, T. Uzer, and Rigoberto Hernandez. Stochastic transition states: Reaction geometry amidst noise. *J. Chem. Phys.*, 123(20):204102, November 2005.
20. Thomas Bartsch, T. Uzer, Jeremy M. Moix, and Rigoberto Hernandez. Transition-state theory rate calculations with a recrossing-free moving dividing surface. *J. Phys. Chem. B*, 112(2):206–212, January 2008.
21. Shinnosuke Kawai, André D. Bandrauk, Charles Jaffé, Thomas Bartsch, Jesús Palacián, and T. Uzer. Transition state theory for laser-driven reactions. *J. Chem. Phys.*, 126(16):164306, April 2007.
22. Ludwig Arnold. *Random Dynamical Systems*. Springer, Berlin, 1998.
23. Shinnosuke Kawai and Tamiki Komatsuzaki. Dynamic pathways to mediate reactions buried in thermal fluctuations. I. Time-dependent normal form theory for multidimensional Langevin equation. *J. Chem. Phys.*, 131(22):224505, 2009.
24. Shinnosuke Kawai and Tamiki Komatsuzaki. Dynamic pathways to mediate reactions buried in thermal fluctuations. II. Numerical illustrations using a model system. *J. Chem. Phys.*, 131(22):224506, 2009.
25. Shinnosuke Kawai and Tamiki Komatsuzaki. Hierarchy of reaction dynamics in a thermally fluctuating environment. *Phys. Chem. Chem. Phys.*, 12:7626–7635, 2010.
26. Shinnosuke Kawai and Tamiki Komatsuzaki. Nonlinear dynamical effects on reaction rates in thermally fluctuating environments. *Phys. Chem. Chem. Phys.*, 12(27):7636–7647, June 2010.
27. H. A. Kramers. Brownian motion in a field of force and the diffusion model of chemical reactions. *Physica (Utrecht)*, 7(4):284–304, April 1940.
28. Eli Pollak and Peter Talkner. Activated rate processes: Finite-barrier expansion for the rate in the spatial-diffusion limit. *Phys. Rev. E*, 47(2):922–933, February 1993.
29. Peter Talkner and Eli Pollak. Numerical test of finite-barrier corrections for the hopping rate in a periodic potential. *Phys. Rev. E*, 47(1):R21–R23, January 1993.
30. P. L. García-Müller, F. Borondo, Rigoberto Hernandez, and R. M. Benito. Solvent-induced acceleration of the rate of activation of a molecular reaction. *Phys. Rev. Lett.*, 101(17):178302, October 2008.
31. Mauro Ferrario and Paolo Grigolini. The non-Markovian relaxation process as a "contraction" of a multidimensional one of Markovian type. *J. Math. Phys.*, 20(12):2567–2572, December 1979.
32. Paolo Grigolini. A generalized Langevin equation for dealing with nonadditive fluctuations. *Journal of Statistical Physics*, 27:283–316, 1982.
33. Fabio Marchesoni and Paolo Grigolini. On the extension of the Kramers theory of chemical relaxation to the case of nonwhite noise. *J. Chem. Phys.*, 78(10):6287–6298, May 1983.
34. Craig C. Martens. Qualitative dynamics of generalized Langevin equations and the theory of chemical reaction rates. *J. Chem. Phys.*, 116(6):2516–2528, February 2002.